

# Chaos in two-dimensional Kepler problem with spin-orbit coupling

V.A. Stephanovich<sup>1</sup> and E.Ya. Sherman<sup>2,3</sup>

<sup>1</sup>*Institute of Physics, Opole University, Opole, 45-052, Poland*

<sup>2</sup>*Department of Physical Chemistry, University of the Basque Country UPV/EHU, 48080 Bilbao, Spain*

<sup>3</sup>*IKERBASQUE Basque Foundation for Science, Bilbao, Spain*

(Dated: July 8, 2021)

We consider classical two-dimensional Kepler system with spin-orbit coupling and show that at a sufficiently strong coupling it demonstrates a chaotic behavior. The chaos emerges since the spin-orbit coupling reduces the number of the integrals of motion as compared to the number of the degrees of freedom. This reduction is manifested in the equations of motion as the emergence of the anomalous velocity determined by the spin orientation. By using analytical and numerical arguments, we demonstrate that the chaotic behavior, being driven by this anomalous term, is related to the system energy dependence on the initial spin orientation. We observe the critical dependence of the dynamics on the initial conditions, where system can enter and exit a stability domain by very small changes in the initial spin orientation. Thus, this system can demonstrate a reentrant order-from-disorder transition driven by very small variations in the initial conditions.

## I. INTRODUCTION

The emergence of a chaotic behavior is one of the most intriguing features of dynamical systems [1–5]. For instance, simple dynamical systems with an energy-dependent separatrix (boundary between qualitatively different trajectories in their phase space), demonstrate chaos, e.g., being driven by a periodic external field.

Dynamical systems with spin-orbit coupling (SOC), ranging from semiconductors [6] to ultracold atomic matter [7, 8], became a topic of a great interest due to rich variety of physical effects observable there. Here we propose and study a class of nonstandard classical *conservative* dynamical systems, which can be characterized as two-dimensional (2D) spin-orbit coupled Kepler systems. We show that inclusion of a new internal degree of freedom, namely, the particle spin, coupled to its momentum, leads to the chaos emergence.

Without SOC, the properties of the above systems are well-known in classical [9] and quantum [10] realization and no chaotic behavior is expected there except a quantum chaos in an applied magnetic field acting at the orbital electron motion [11]. Three integrals of motion: the energy, the angular momentum, and the Runge-Lenz vector fully determine the dynamics of the system and assure its stability against chaos. The SOC introduces new degrees of freedom and lowers the system symmetry to the existence of only two integrals of motion. This symmetry reduction can be seen as a SOC-generated spin-dependent contribution to the velocity proportional to the SOC constant. As a result, the system loses integrability due to the spin back action on the orbital motion and can demonstrate a chaotic behavior close to the separatrix which determines the boundary between a finite and a delocalized motion.

An experimentally realizable example of such a system is given by 2D excitons in semiconductor structures [12–14]. We shall consider the classical limit of orbital motion corresponding to the highly excited Rydberg states of these excitons. Recently, it has been experimentally es-

tablished that lowering of the system symmetry from the vacuum  $SO(4)$  to the discrete symmetry of a host crystal for three-dimensional excitons leads to a chaos even in the SOC absence [15–17]. Using only classical arguments, here we prove that the spin-orbit coupling, being a lower-symmetry contribution to the system dynamics, can induce the chaotic motion.

Two aspects of SOC-related randomness have recently been studied in two-dimensional harmonic potentials, where particle's motion is always finite. Larson *et al.* [18] studied thermalization in cold atomic gases in the presence of anisotropic SOC, while Marchukov *et al.* [19] examined the spectral properties in terms of the ensembles emerging in the random matrix theory. In addition, a chaos-like behavior in driven SOC systems with a strong confinement has been considered in Refs. [20] and [21]. Conservative two-dimensional systems with interaction potentials vanishing at large distances, being augmented by the SOC, provide nontrivial examples of a classical chaotic behavior, qualitatively different from above settings. Motivated by possible transitions to the nontrivial chaotic behavior, here we study the effects of weak and strong SOC on the dynamics of a Kepler-like system, prove that such transitions indeed occur, and analyze different regimes of the chaotic motion.

This paper is organized as follows. In Section II we introduce general equations and integrals of motion for the Kepler system with spin-orbit coupling. In Section III we perform perturbative analysis of the trajectories at a weak SOC. In Section IV the chaotic behavior at a sufficiently strong SOC will be presented and analyzed. Conclusions and relation to possible experiments will be given in Section V.

## II. EQUATIONS AND INTEGRALS OF MOTION

We take the minimal Hamiltonian describing the 2D Kepler problem with SOC in the form  $H = H_0 + H_{\text{so}}$ .

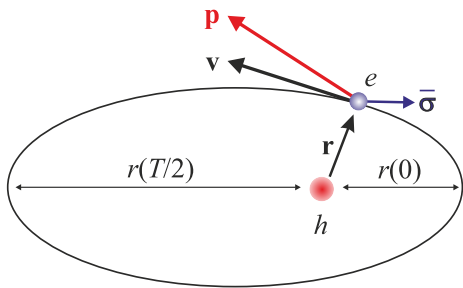


FIG. 1. Single-period trajectory with  $\bar{\sigma}_x = 1$  at a weak SOC. Notations correspond to the text. Electron ( $e$ ) starts to move at the distance  $r(0)$  from the fixed hole ( $h$ ) and at  $t = T/2$ , where  $T$  is the rotation period, reaches the distance  $r(T/2)$ .

The spin-independent part is:

$$H_0 = \frac{p^2}{2m} - \frac{e^2}{r}, \quad (1)$$

where  $\mathbf{r} = (x, y)$  is the electron coordinate,  $\mathbf{p}$  is the electron momentum (see Fig. 1),  $m$  is its mass, and  $e$  is the effective charge including the dielectric constant of a host crystal. We take the SOC term in the Rashba form [22] with rotational symmetry of the spectrum:

$$H_{\text{so}} = \frac{\alpha}{\hbar} (p_x \sigma_y - p_y \sigma_x), \quad (2)$$

with  $\alpha$  being the coupling constant [24] and  $\sigma_i$  are the Pauli matrices corresponding to spin  $1/2$ . This type of coupling appears as a result of either spatial inversion asymmetry in solids [22, 23] or can be generated optically in cold atomic gases [7, 8].

Although here we concentrate on the classical dynamics, it is instructive to make a connection with the quantum approach. Namely, we consider a system with two-component wavefunction in the form:

$$\psi(\mathbf{r}, t) = \varphi(\mathbf{r}, t) \begin{bmatrix} \cos(\theta/2) e^{i\phi} \\ \sin(\theta/2) \end{bmatrix}. \quad (3)$$

Here  $\varphi(\mathbf{r}, t)$  is the (spatial and temporal dependent) wavepacket-like envelope function and time-dependent angles  $\theta$  and  $\phi$  determine spin components as:

$$\sigma_z = \cos \theta, \quad \sigma_x = \sin \theta \cos \phi, \quad \sigma_y = -\sin \theta \sin \phi. \quad (4)$$

Subsequently we assume the classical limit for orbital motion, while the spin remains quantum. To be specific, here we characterize the orbital motion by the classical coordinate  $\mathbf{r}$  and momentum  $\mathbf{p}$ , whereas *quantum* spin defines the momentum-dependent precession [18, 23] and related to this precession effects, as described below.

The characteristic feature of Hamiltonian (2) is the anomalous spin-dependent velocity [25] (see Fig. 1) presented in the commutator form  $\mathbf{v}_{\text{so}} \equiv i[H_{\text{so}}, \mathbf{r}]/\hbar = \alpha(\sigma_y, -\sigma_x)/\hbar$ . Two other SOC characteristics [23] of our interest are the spin precession with the rate  $2p\alpha/\hbar^2$

and the corresponding length  $l_{\text{so}} = \hbar^2/m\alpha$ , necessary for electron to essentially rotate the spin.

To formulate the classical equations of motion, we observe from Eq. (2) that the above anomalous velocity is the derivative  $\mathbf{v}_{\text{so}} = \partial H_{\text{so}}/\partial \mathbf{p}$ . For Hamiltonian function  $H = H_0 + H_{\text{so}}$  these equations can be obtained by substituting the spin components in Eq. (2) by their expectation values  $\bar{\sigma}_i$  such that  $\bar{\sigma}_x^2 + \bar{\sigma}_y^2 + \bar{\sigma}_z^2 = 1$ . This yields

$$\dot{\mathbf{p}} = -e^2 \frac{\mathbf{r}}{r^3}, \quad \dot{\mathbf{r}} = \frac{\mathbf{p}}{m} - \frac{\alpha}{\hbar} [\mathbf{z} \times \bar{\boldsymbol{\sigma}}], \quad (5)$$

where  $\mathbf{z} = (0, 0, 1)$  is the unit vector perpendicular to ( $xy$ ) plane, where the motion occurs. The equations for spin components corresponding to the precession dependent on the particle momentum read:

$$\begin{aligned} \dot{\bar{\sigma}}_x &= 2 \frac{\alpha m}{\hbar^2} \left( \dot{x} - \frac{\alpha}{\hbar} \bar{\sigma}_y \right) \bar{\sigma}_z, \\ \dot{\bar{\sigma}}_y &= -2 \frac{\alpha m}{\hbar^2} \left( \dot{y} + \frac{\alpha}{\hbar} \bar{\sigma}_x \right) \bar{\sigma}_z, \\ \dot{\bar{\sigma}}_z &= -2 \frac{\alpha m}{\hbar^2} (\dot{x} \bar{\sigma}_x + \dot{y} \bar{\sigma}_y). \end{aligned} \quad (6)$$

Equations (5) and (6) permit the complete classical analysis of particle position and spin components time dependence [26]. Their direct iterative and exact numerical solutions will be used for the description of the trajectories.

Integrals of motion in this system are the energy  $E$ , the  $z$ -component of total angular momentum  $\hbar(L + \bar{\sigma}_z/2) \equiv p_y x - p_x y + \hbar \bar{\sigma}_z/2$  and the length of the spin vector  $\bar{\sigma}^2 = 1$ . The above conservation laws can be verified by direct calculation. The conservation of spin vector length is due to the spin precession with the tip moving over the Bloch sphere. Note that there is no integral of motion corresponding to the Runge-Lenz vector specific for the Coulomb-like field in the Kepler problem without spin-orbit coupling. Then, with the SOC included, the system having five coupled degrees of freedom, possesses only three integrals of motion. As a result, it exhibits an unusual chaotic behavior as we shall see below.

Since the comprehensive description of the Kepler trajectories can be done with the  $t = 0$  initial conditions

$$\mathbf{r}(0) = (r_0, 0), \quad \mathbf{p}(0) = (0, p_0), \quad (7)$$

we employ these conditions for subsequent analysis. We will measure the energy in  $e^2/r_0$  and momentum in  $e\sqrt{m/r_0}$  units respectively. The condition for the system to be in a highly excited Rydberg state is  $r_0 \gg \hbar^2/m e^2$ . In addition, in what follows we put  $\hbar = m = e = 1$ . In Eq. (7),  $p_0^2/2 - 1 \equiv E_0$  is the initial energy in the SOC absence, which determines the trajectory shape. In this case, the initial angular momentum  $L(0) \equiv \sqrt{2(1 + E_0)}$ . Note that  $E_0 = -1/2$  determines the special case of circular trajectory. Its special character will be demonstrated below. The total conserved energy is  $E = E_0 - \alpha p_0 \bar{\sigma}_x(0)$ . We will vary the initial conditions by modifying the initial

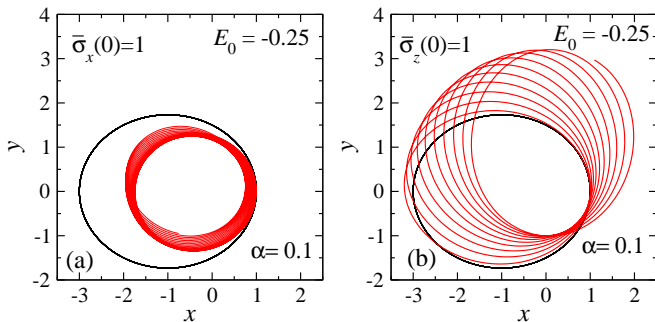


FIG. 2. Trajectories for  $E_0 = -0.25$  and initial spins  $\bar{\sigma}_x(0) = 1$  (a) and  $\bar{\sigma}_z(0) = 1$  (b). In both panels  $\alpha = 0.1$ . Elliptic line is the trajectory for  $\alpha = 0$ .

spin:  $\bar{\sigma}(0) = (\bar{\sigma}_x(0), \bar{\sigma}_y(0), \bar{\sigma}_z(0))$  and study the subsequent coupled spin-coordinate motion dependent on the initial spin vector. We shall demonstrate numerically that at sufficiently large  $\alpha$  the chaotic trajectories emerge in the system under consideration.

### III. WEAK SPIN-ORBIT COUPLING: TRAJECTORY DEFORMATION

We begin with the solution of equations of motion to describe the trajectories at weak SOC. Here we can study the dynamics by iterative procedure in  $\alpha$  in Eqs. (5), (6) with the elliptic Kepler trajectory and time-independent spin as zero-order approximation. In this case the anomalous velocity has two main effects on the trajectory shape: (i) it shifts the position of the point  $r(T/2)$  (see Fig. 1) and (ii) it rotates the entire trajectory (see Appendix A for details). Based on the total angular momentum and energy conservation, we present the position of the particle at  $t = T/2$  as:

$$r(T/2) = \frac{L^2(T/2)}{Z_{T/2} \mp \sqrt{Z_{T/2}^2 + 2EL^2(T/2)}}, \quad (8)$$

where  $Z_{T/2} \equiv 1 - \alpha L(T/2)\bar{\sigma}_x(T/2)$ ,  $L(T/2) \equiv L(0) + \Delta_z$ ,  $2\Delta_z \equiv \bar{\sigma}_z(0) - \bar{\sigma}_z(T/2)$ , and the upper (lower) sign corresponds to  $E_0 > -1/2$  ( $E_0 < -1/2$ ). At  $\alpha = 0$  we have  $r(T/2) = R$ , where  $R \equiv -(E_0 + 1)/E_0$  determines the limit of the trajectory in the absence of the SOC, and at finite  $\alpha$ , we consider the shift  $r(T/2) - R$ . Analysis of Eq. (8) shows that  $E_0 = -1/2$ , where  $1 + 2E_0L^2(0) = 0$ , is the special case (see Appendix A for details), which should be considered separately. To demonstrate the key role of the initial conditions, we consider two cases which are strongly different in terms of the anomalous initial velocity.

We begin with  $\bar{\sigma}_x(0) = 1$ , where the initial velocity is  $\mathbf{v}(0) = (0, p - \alpha)$ . The first two iterations of Eqs. (5), (6) yield the leading terms in the spin components  $\bar{\sigma}_z(T/2) = 2\alpha(R + 1)$  and  $\bar{\sigma}_x(T/2) = 1 - 2\alpha^2(R + 1)^2$ . It

is seen that the main contribution in Eq. (8) comes from  $\bar{\sigma}_z(T/2)$ , which is linear in  $\alpha$ , and we may safely disregard the  $\sim \alpha^2$  correction in  $\bar{\sigma}_x(T/2)$ . Then, at  $|1 + 2E_0| \gg \alpha$ , the linear in  $\alpha$  correction to the position becomes:

$$R - r(T/2) = -\frac{R}{l_{\text{so}}} \frac{1}{E_0} \frac{\sqrt{2}}{\sqrt{1 + E_0}}. \quad (9)$$

The initial condition  $\bar{\sigma}_z(0) = 1$  can be considered along the same lines with  $\mathbf{v}(0) = (0, p_0)$  and  $E = E_0$ . We obtain two main contributions to the shape of the trajectory:  $\bar{\sigma}_x(T/2) = -2(R + 1)/l_{\text{so}}$  and  $\bar{\sigma}_z(T/2) = 1 - 2(R + 1)^2/l_{\text{so}}^2$ , resulting at  $|1 + 2E_0| \gg \alpha^2$  in

$$R - r(T/2) = -\frac{R(R + 1)}{l_{\text{so}}^2} \frac{\sqrt{2}}{\sqrt{1 + E_0}}. \quad (10)$$

To illustrate the deformation of the trajectories, in Fig. 2, we present them at a moderate SOC for different initial conditions. The shapes of the trajectories correspond well to Eqs. (9) and (10). At a sufficiently strong SOC, corresponding to a small  $l_{\text{so}}$ , the relevant quantities such as deformations and rotations, become large, providing a hint to possible chaotic behavior.

### IV. CHAOS AND ORDER FROM DISORDER AT STRONG COUPLING

Having discussed the effect of the relatively weak and moderate SOC, we can establish a crossover from the weak to a strong coupling regime. The qualitative effects of strong SOC appear when  $\alpha$  becomes of the order of the minimal Kepler velocity,  $v_{\text{min}}$ . For simplicity we consider the case  $E_0 \rightarrow -0$ . In this limit  $R = 1/|E_0|$  and  $L(0) = \sqrt{2}$ , therefore,  $v_{\text{min}} = \sqrt{2}|E_0|$  and the criterion of strong SOC becomes  $\alpha \gtrsim |E_0|$ . However, there is a subtle effect related to the role of the initial conditions - if the anomalous velocity is initially zero, as in the  $\bar{\sigma}_z(0) = 1$  case, it needs some time to be developed. Taking into account that the spin precession yields  $\bar{\sigma}_x(T/2) \sim \alpha R$ , here the condition of an immediate strong effect of SOC, becomes  $\alpha^2 R \sim |E_0|$ .

Now we can determine the critical value  $\alpha_c$ , which permits ionization of the initial state and serves as a typical SOC value where the chaotic regime can be seen. The minimum of the SOC (2) eigenenergy  $E = -\alpha^2/2$  occurs at  $p = \alpha$ , and the ionization is determined by the condition that the total energy  $E = E_0 - \alpha_c p_0 \bar{\sigma}_x(0)$  equals to the SOC eigenenergy minimum

$$E_0 - \alpha_c p_0 \bar{\sigma}_x(0) = -\frac{\alpha_c^2}{2}. \quad (11)$$

The solution of Eq. (11) yields  $\alpha_c = u_0 + \sqrt{u_0^2 - 2E_0}$ , where  $u_0 = p_0 \bar{\sigma}_x(0)$ , demonstrating a non-analytical dependence of  $\alpha_c$  on the initial conditions.

For  $\bar{\sigma}_x(0) = 0$  it is immediately seen that  $\alpha_c = \sqrt{2|E_0|}$ , and this condition is stronger than  $\alpha \gtrsim |E_0|$ .

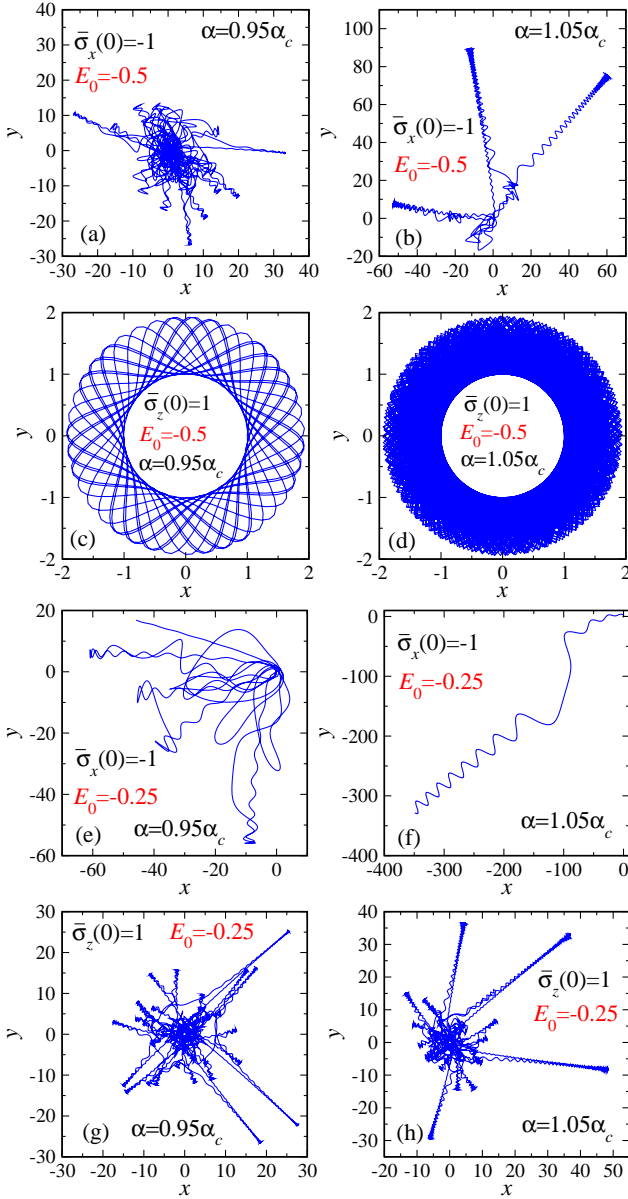


FIG. 3. The electron trajectories in the exciton with SOC for energies  $E_0 = -0.5$  ((a)-(d)) and  $E_0 = -0.25$  ((e)-(h)) for the parameters shown in the panels. Left and right columns correspond to  $\alpha = 0.95\alpha_c$  and  $\alpha = 1.05\alpha_c$ , respectively. Here  $\alpha_c = \sqrt{2}(1 - \sqrt{1 + E_0})$  for  $\bar{\sigma}_x(0) = -1$  and  $\alpha_c = \sqrt{-2E_0}$  for  $\bar{\sigma}_z(0) = 1$ . Panels (c) and (d) demonstrate that these initial conditions belong to a domain of stability with respect to SOC-induced chaotization. In all the panels except (c), time  $t < 10^3$ ; in the panel (c)  $t < 2 \cdot 10^2$  for a better resolution of the trajectory.

Therefore, even when the trajectory is strongly modified by the Rashba coupling, the motion can still be finite. This difference can be seen in the opposite limit as well:  $E_0 \rightarrow -1$  yields  $p_0 \rightarrow 0$  with  $\alpha_c = \sqrt{2} \gg p_0$ .

We now address the possibility of occurrence of infinite trajectories, that is of the exciton ionization, at a given

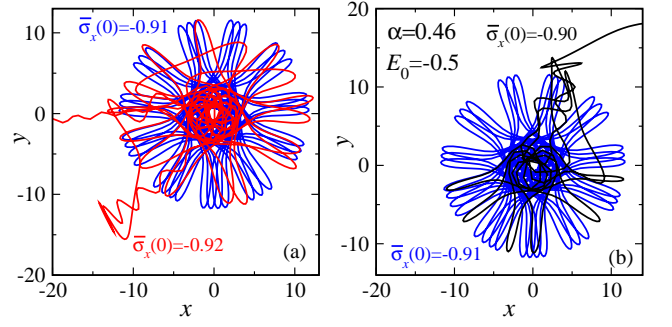


FIG. 4. Trajectories at different initial spins marked near the lines for the parameters shown in the panel (b). Note that at  $\bar{\sigma}_x(0) = -0.91$  the trajectory is flower-like (as presented for  $t < 2 \times 10^2$ ). Here initial spin rotates in the  $(xz)$  plane such that  $\bar{\sigma}_y(0) = 0$ .

$\alpha$ . To create such a trajectory (which is a consequence of the initial bound state ionization), one needs  $\bar{\sigma}_x(0) < \bar{\sigma}_x^{cr}(0) \equiv (E_0 + \alpha^2/2)/\alpha p_0$ . This equation determines the minimal value of  $\alpha_c$ , corresponding to  $\bar{\sigma}_x(0) = -1$ :

$$\alpha_c^{\min} = -p_0 + \sqrt{p_0^2 - 2E_0} = \sqrt{2} \left( 1 - \sqrt{1 + E_0} \right). \quad (12)$$

At smaller  $\alpha < \alpha_c^{\min}$  the motion is always finite and the SOC-induced ionization is prohibited.

Therefore, if the total initial energy of the system approaches  $-\alpha^2/2$  from below, the particle shows a finite but long-range motion with the maximal distance  $r_{\max} \sim (\alpha_c - \alpha)^{-1}$ . In contrast to the conventional Kepler problem, where the motion remains elliptic when the negative total energy approaches zero, here it can become chaotic. In general, condition  $E = -\alpha^2/2$  determines a multidimensional separatrix in the phase space augmented by spin subspace. Note that ionization condition  $E > -\alpha^2/2$  is a necessary, but not sufficient one - even when it is satisfied, the motion can still be finite, making a qualitative difference from the behavior without SOC. Indeed, at  $\alpha = 0$ , when  $L$  is the integral of motion, the dynamics can be reduced to one-dimensional form with the effective potential energy  $U_{\text{eff}}(r) = -1/r + L^2/2r^2$  [9] explicitly including  $L$ . This one-dimensional mapping results in  $E_0 > 0$  being both the necessary and sufficient condition for the ionization. For nonzero  $\alpha$  such a mapping cannot be done and the condition  $E_0 > -\alpha^2/2$  is not sufficient anymore.

Now we provide evidence for the chaotic behavior based on numerical solutions of Eqs. (5) and (6). The particle trajectories near the separatrix corresponding to the critical SOC are presented in Fig. 3, demonstrating a variety of behaviors. The minimal and maximal distance reached by the particle in this case are determined by the conservation laws. Figure 3, demonstrating all possible behaviors of the SOC-augmented Kepler problem close to the critical coupling, can be considered as the main result of our analysis. These behaviors include:



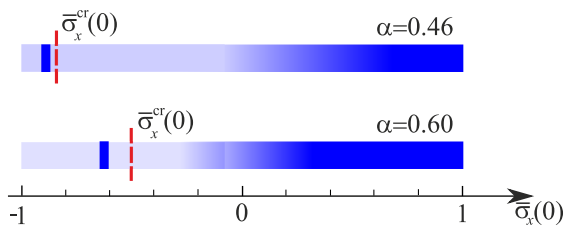


FIG. 5. Different regimes of motion dependent on the initial spin component  $\bar{\sigma}_x(0)$  exemplified by  $xz$ -plane rotation for  $\alpha = 0.46$  and  $0.6$ . In this case  $\bar{\sigma}_y(0) = 0$  and  $\bar{\sigma}_z(0) = \sqrt{1 - \bar{\sigma}_x^2(0)}$ . Dark (blue in color version) parts correspond to a regular finite motion, while gray (light blue) parts correspond to chaotic one, either localized or delocalized. Thus, the bars show a gradual development of the chaos-related features following the regular motion. The necessary condition (boundary, dashed vertical lines) for ionization is given by  $\bar{\sigma}_z^{\text{cr}}(0)$  defined above Eq. (12) with  $\bar{\sigma}_z^{\text{cr}}(0) = -0.86$  and  $\bar{\sigma}_x^{\text{cr}}(0) = -0.53$  for  $\alpha = 0.46$  and  $\alpha = 0.6$  respectively. A narrow domain of a regular motion appears at  $\bar{\sigma}_x(0) < \bar{\sigma}_x^{\text{cr}}(0)$ . These domains are determined by  $\bar{\sigma}_x(0) \in (-0.915, -0.905)$  and  $\bar{\sigma}_x(0) \in (-0.64, -0.6)$  for  $\alpha = 0.46$  and  $\alpha = 0.6$  respectively.

1) strongly entangled chaotic trajectories with "protuberances" in Figs. 3(a), (b), (e), (g), and (h), as expected from the fact that the number of the integrals of motion is less than the number of the degrees of freedom;

2) stable unperiodic orbits filling regular ring-like areas in the  $(xy)$ -plane in Figs. 3(c) and (d). This behavior resembles the trajectories in a system with a non-Coulomb potential  $U(r)$  as presented, e.g., in Ref. [9], demonstrating a stability point in the Kepler problem with SOC, and

3) relatively simple trajectories corresponding to the exciton ionization in Fig. 3(f).

At large distances,  $r \gg \pi l_{\text{so}}$ , the influence of Coulomb potential on the velocity is negligible compared to that of the spin-orbit coupling. Hence, in this case the electron motion is almost completely defined by SOC. Latter fact permits analytical description of both the trajectories like rare protuberances, where electron still returns to the chaotic region with  $r \lesssim \pi l_{\text{so}}$ , and ionization ones with  $r \rightarrow \infty$ . Without loss of generality, here we concentrate on the case of the particle characterized by weakly time-dependent momentum, which we consider for definiteness to be constant in time as  $\mathbf{p} = p(\cos \theta, \sin \theta)$ . The total energy now consists of two constant terms: the kinetic energy  $p^2/2$  and the SOC-related contribution

$$\epsilon_{\text{so}} = \alpha(p_x \bar{\sigma}_y(0) - p_y \bar{\sigma}_x(0)). \quad (13)$$

Hence, the precession of the SOC-induced spin component parallel to the momentum  $\mathbf{p}\bar{\sigma}$  reads:

$$\mathbf{p}\bar{\sigma}(\tilde{t}) = \mathbf{p}\bar{\sigma}(0) \cos(2\alpha p \tilde{t}), \quad \tilde{t} \equiv t - t_0, \quad (14)$$

where  $t_0$  is the initial time for the constant- $p$  motion. By solving these equations we obtain the velocities  $v_x(\tilde{t}) =$

$$p_x + \alpha \bar{\sigma}_y(\tilde{t}) \quad \text{and} \quad v_y(\tilde{t}) = p_y - \alpha \bar{\sigma}_x(\tilde{t}):$$

$$\begin{aligned} v_x(\tilde{t}) &= p_x + \alpha \left[ \bar{\sigma}_y(\tilde{0}) f_1(\tilde{t}) - \bar{\sigma}_x(\tilde{0}) f_2(\tilde{t}) \right], \\ v_y(\tilde{t}) &= p_y - \alpha \left[ \bar{\sigma}_x(\tilde{0}) f_3(\tilde{t}) - \bar{\sigma}_y(\tilde{0}) f_2(\tilde{t}) \right], \end{aligned} \quad (15)$$

where  $f_1(t) = 1 - 2 \sin^2 \theta \sin^2 \phi$ ,  $f_2(t) = \sin 2\theta \sin^2 \phi$ , and  $f_3(t) = 1 - 2 \cos^2 \theta \sin^2 \phi$  with  $\phi \equiv \alpha p t$ . As we can see from Eqs.(15), the motion has an oscillatory character corresponding to Fig. 3.

Equations (15) have an interesting limit. Consider particle with momentum  $p = \alpha$ . Then, the energy  $E = \alpha^2/2 + \alpha^2(\cos \theta \bar{\sigma}_y(0) - \sin \theta \bar{\sigma}_x(0))$  has the minimum  $E = -\alpha^2/2$  at  $\bar{\sigma}_y(0) = -\cos \theta$ ,  $\bar{\sigma}_x(0) = \sin \theta$ . Slightly away from the minimum by taking:  $\bar{\sigma}_y(0) = -\cos(\theta + \eta)$ ,  $\bar{\sigma}_x(0) = \sin(\theta + \eta)$  with small  $\eta \ll 1$  we obtain  $v_x = \alpha \eta \sin \theta \cos(2\alpha^2 t)$  and  $v_y = -\alpha \eta \cos \theta \cos(2\alpha^2 t)$ . Here the nonzero velocity appears only due to deviation of the energy from  $-\alpha^2/2$  with  $E = -\alpha^2(1 - \eta^2)/2$ . This corresponds to small but fast oscillations in the "protuberances" in Fig. 3. These oscillations are an extreme manifestation of a *Zitterbewegung* [27, 28] typical for spin-orbit coupled systems.

An important characteristic feature of a chaotic motion such as strong dependence on the initial conditions is presented in Fig. 4. It clearly demonstrates a transition from chaotic to confined regular trajectory (Fig. 4(a)) in the stability domain and *vice versa* (Fig. 4(b)) at small variations in the initial spin direction. The stability point here is approximately  $\bar{\sigma}_x(0) = -0.91$ . Note that the chaotic trajectories reported in Fig. 4(a) and (b) (corresponding to  $\bar{\sigma}_x(0) = -0.9$  and  $0.92$  respectively) are qualitatively similar to those in Fig. 3(b) since the value of  $\alpha$  is larger than the critical  $\alpha_c$  obtained with Eq. (11) for both initial spin orientations.

In general, the trajectory shape depends on the SOC strength and the entire set of the initial conditions, making the analysis very cumbersome. To obtain a semi-quantitative pattern of different regimes of the motion, the domain of initial conditions in Fig. 4 can be extended to the entire  $\bar{\sigma}_x(0) = (-1, 1)$  domain. The results are presented in Fig. 5 for two values of the constant  $\alpha$ . This Figure shows a gradual development of chaos-related features such as increasing entanglement of the trajectories and length of the protuberances following the regular behavior and can be regarded as a "stability diagram" of the system under consideration. Another important feature, which already follows from Fig. 4, is a reentrance of regular trajectories from chaotic ones and *vice versa* near the threshold values  $\bar{\sigma}_x^{\text{cr}}(0)$ . Latter effect can be considered as "order from disorder" driven by variation in the initial spin direction.

## V. CONCLUSIONS

We have studied the emergence of chaos in the classical Kepler problem with the Rashba spin-orbit coupling. Such systems can be experimentally realized, for

instance, in highly excited Rydberg-like states of two-dimensional excitons in semiconductor structures. At a weak Rashba coupling, corresponding to small interaction constants  $\alpha$ , the elliptic Kepler trajectories are modified in shape and orientation and densely fill a part of the particle motion plane. This behavior is somewhat similar, although not identical, to that of the Kepler problem trajectories in the potentials  $-1/r^b$ , where  $b > 0$  and  $b \neq 1$  [9]. With the increase in  $\alpha$ , the deformations of the trajectories become strong and in the vicinity of the critical  $\alpha_c$  corresponding to the exciton breakdown, the trajectories can become chaotic. Typical chaotic trajectory can be described as a highly entangled path in the vicinity of the initial position with rare long protuberances increasing in length at approaching the ionization threshold. At a sufficiently large  $\alpha$ , the SOC assisted ionization becomes possible and the bound state disappears. The reason for the chaos lies in the fact that the system lost integrability since it possesses only two integrals of motion for its four degrees of freedom. Dynamically, this effect is clearly seen in the equations of motion including the anomalous spin-dependent velocity term.

As typical for a chaotic system, its dynamics exhibits a critical dependence on the initial conditions, demonstrating the transition from a chaotic to a regular behavior and *vice versa* caused by very small variations in the initial spin orientation. The latter feature could be referred to as reentrant "order-from-disorder" transition. Our results can have important implications for the properties of semiclassical Rydberg-like states of excitons in two-dimensional structures, where a chaotic regime due to spin-orbit coupling may be developed.

To make relation to possible observations, we mention that the typical energies of highly excited Rydberg 2D ex-

citons in semiconductor quantum wells are of the order of 0.1 meV and the size is around 100 nm [29]. Therefore, a typical length of the chaotic protuberances is about  $10^3$  nm (1  $\mu\text{m}$ ) and a typical time the electron spends in a long protuberance is about a nanosecond. We mention here several realizations, where predicted chaotic trajectories can play a role. For example, they can be relevant for interaction between distant 2D excitons. Indeed, the long-range chaotic trajectories presented in Fig. 3 are characterized by large dipole moments  $\mathbf{er}(t)$ , enhancing long-range electric fields of the excitons. The chaotic trajectories of electrons from different excitons can interlace, which alters the exciton-exciton interaction leading either to their ionization or to a modified lateral motion. In addition, this chaotic behavior can strongly influence relaxation of electron energy in the Rydberg excitons by emission of phonons. Instead of a process with well-defined time dependence, the energy relaxation from a highly excited to the ground state may become chaotic and largely unpredictable. Moreover, the electrons at those remote trajectories, can eventually be trapped in distant electrostatic fields (e.g. Ref. [30]) or at the system boundaries.

#### ACKNOWLEDGMENTS

E.Y.S. acknowledges the support by the Spanish Ministry of Economy, Industry, and Competitiveness and the European Regional Development Fund FEDER through Grant No. FIS2015-67161-P (MINECO/FEDER), and Grupos Consolidados UPV/EHU del Gobierno Vasco (IT-986-16).

#### Appendix A: Trajectory shape at weak spin-orbit coupling

Based on the energy and angular momentum conservation, we calculate the particle's position at  $t = T/2$ . At this time instant, the energy can be written as:

$$E = \frac{p^2(T/2)}{2} + \alpha p(T/2) \bar{\sigma}_x(T/2) - \frac{1}{r(T/2)}, \quad p(T/2) = \frac{L(T/2)}{r(T/2)}. \quad (\text{A1})$$

The total angular momentum conservation yields  $L(T/2) = L(0) + (\bar{\sigma}_z(0) - \bar{\sigma}_z(T/2))/2$ . Thus, we obtain:

$$\frac{(L(0) + \Delta_z)^2}{r^2(T/2)} + \frac{2}{r(T/2)} (\alpha(L(0) + \Delta_z) \sigma_x(T/2) - 1) - 2E = 0, \quad (\text{A2})$$

where  $\Delta_z \equiv (\bar{\sigma}_z(0) - \bar{\sigma}_z(T/2))/2$ . The solution of (A2) with respect to  $r(T/2)$  yields

$$r(T/2) = \frac{(L(0) + \Delta_z)^2}{1 - \alpha(L(0) + \Delta_z) \bar{\sigma}_x(T/2) \mp \sqrt{(\alpha(L(0) + \Delta_z) \bar{\sigma}_x(T/2) - 1)^2 + 2E(L(0) + \Delta_z)^2}}, \quad (\text{A3})$$

where upper (lower) sign corresponds to  $E_0 > -1/2$  ( $E_0 < -1/2$ ). This equation is tantamount to Eq. (8) of the main text.

Now we apply Eq. (A3) to the initial conditions  $\bar{\sigma}_x(0) = 1$ , where  $E = E_0 - \alpha\sqrt{2(1 + E_0)}$ , and  $L(0) = \sqrt{2(1 + E_0)}$ . The equations for spin precession with respect to anomalous velocity read:

$$\dot{\bar{\sigma}}_x = 2\alpha(v_x - \alpha\bar{\sigma}_y)\bar{\sigma}_z; \quad \dot{\bar{\sigma}}_y = -2\alpha(v_y + \alpha\bar{\sigma}_x)\bar{\sigma}_z; \quad \dot{\bar{\sigma}}_z = -2\alpha(v_x\bar{\sigma}_x + v_y\bar{\sigma}_y). \quad (\text{A4})$$

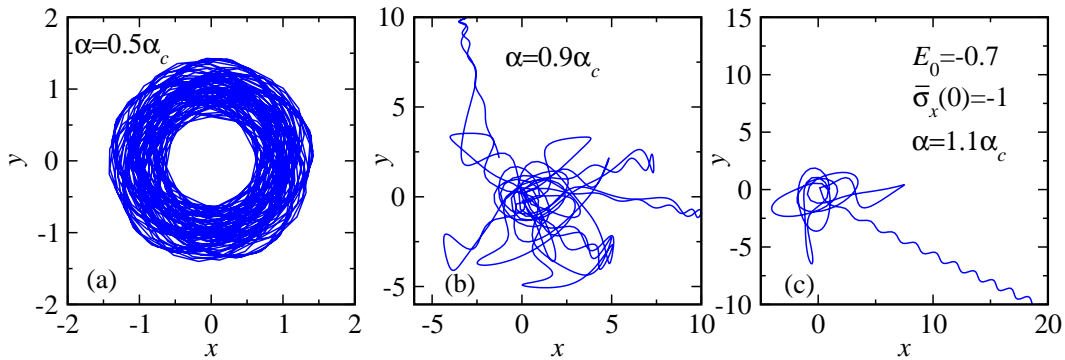


FIG. 6. Particle trajectory for different values of SOC constant as shown in the panels. (a) Moderate  $\alpha$  with the trajectory filling the allowed part of the  $(xy)$  plane, (b) a chaotic trajectory at  $\alpha$  close to but smaller than the critical value, and (c) ionization trajectory at  $\alpha > \alpha_c$ . In all panels  $E_0 = -0.7$  and initial spin  $\bar{\sigma}_x(0) = -1$ .

We begin with the time dependence of  $\bar{\sigma}_z(t)$  and obtain

$$\bar{\sigma}_z(t) = -2\alpha(x(t) - x(0)) \equiv -2\alpha(x(t) - 1), \quad (\text{A5})$$

resulting in  $\bar{\sigma}_z(T/2) = 2\alpha(R+1)$  and  $L(T/2) = L(0) - \sigma_z(T/2)/2 = L - \alpha(R+1)$ . Second iteration yields  $\bar{\sigma}_x(T/2) = 1 - 2(\alpha(R+1))^2$ , providing the contribution which is not important for the linear in  $\alpha$  approximation. Assuming  $E_0 > -1/2$ , for this case we obtain

$$r(T/2) = \frac{(L(0) - \alpha(R+1))^2}{1 - \alpha(L(0) - \alpha(R+1)) - \sqrt{(\alpha(L(0) - \alpha(R+1)) - 1)^2 + 2E(L(0) - \alpha(R+1))^2}}. \quad (\text{A6})$$

Equation (9) of the main text immediately follows from the above Eq. (A6).

Now we express  $(\alpha(L(0) - \alpha(R+1)) - 1)^2 + 2E(L(0) - \alpha(R+1))^2$  in terms of the energy  $E_0$  and obtain

$$\begin{aligned} & (\alpha(L(0) - \alpha(R+1)) - 1)^2 + 2E(L(0) - \alpha(R+1))^2 = \\ & = (1 + 2E_0)^2 - 2\alpha L(0)(1 + 2E_0) + \alpha^2 \left( \sqrt{2(1 + E_0)} - 8\frac{1 + E_0}{E_0} \right) + \mathcal{O}(\alpha^3). \end{aligned} \quad (\text{A7})$$

Therefore, at  $1 + 2E_0 = 0$ , the corresponding circular trajectory cannot be treated perturbatively and the condition  $|1 + 2E_0| \gg \alpha$  is required for the applicability of the perturbation theory at given  $\alpha \ll 1$ .

### Appendix B: Trajectories at $E_0 < -1/2$ .

In the main text, we have considered three principal realizations of trajectories with  $E_0 \geq -1/2$  as shown in Fig.3 there. Here we complement the corresponding analysis by typical results for  $E_0 < -1/2$  at different values of the SOC constant. Figure 6 shows that the behavior of trajectories corresponds to the chaos emergence near the critical  $\alpha_c = \sqrt{2}(1 - \sqrt{1 + E_0})$ , followed by exciton ionization with  $\alpha$  increase. This result follows from the general analysis in the main text.

- 
- [1] M. C. Gutzwiller, *Chaos in Classical and Quantum Mechanics* (Springer-Verlag, New York, 1990).  
 [2] L. E. Reichl, *The Transition to Chaos. Conservative Classical Systems and Quantum Manifestations*, 2nd ed. (Springer-Verlag, New York, 2004).

- [3] F. Haake, *Quantum Signatures of Chaos*, 3rd ed. (Springer-Verlag, Berlin/Heidelberg, 2010).  
 [4] H.-J. Stöckmann, *Quantum Chaos: An Introduction* (Cambridge University Press, Cambridge, U.K., 1999).  
 [5] *Classical and Quantum Hamiltonian Systems*, edited by

- H. Araki, Lecture Notes in Physics Vol. 93 (Springer-Verlag, Berlin, 1979).
- [6] *Spin Physics in Semiconductors* Springer Series in Solid-State Sciences, Ed. by M. I. Dyakonov, Springer (2008).
- [7] V. Galitski and I. B. Spielman, *Nature* **494**, 49 (2013).
- [8] H. Zhai, *Int. J. Mod. Phys. B* **26**, 1230001 (2012).
- [9] L. D. Landau and E.M. Lifshitz, *Classical Mechanics*, Third Edition: Volume 1 (Course of Theoretical Physics (1976).
- [10] D.G.W. Parfitt and M.E. Portnoi, *Journ. of Math. Phys.* **43**, 4681 (2002).
- [11] H. Friedrich and H. Wintgen, *Physics Reports* **183**, 37 (1989).
- [12] M. V. Durnev and M. M. Glazov, *Phys. Rev. B* **93**, 155409 (2016)
- [13] D. V. Vishnevsky, H. Flayac, A. V. Nalitov, D. D. Solnyshkov, N. A. Gippius, and G. Malpuech, *Phys. Rev. Lett.* **110**, 246404 (2013).
- [14] A. A. High, A. T. Hammack, J. R. Leonard, S. Yang, L. V. Butov, T. Ostatnický, M. Vladimirova, A. V. Kavokin, T. C. H. Liew, K. L. Campman, and A. C. Gossard, *Phys. Rev. Lett.* **110**, 246403 (2013).
- [15] M. Aßmann, J. Thewes, D. Fröhlich, and M. Bayer, *Nat. Mater.* **15**, 741 (2016).
- [16] E. A. Ostrovskaya and F. Nori, *Nat. Mater.* **15**, 702 (2016).
- [17] F. Schweiner, J. Main, and G. Wunner, *Phys. Rev. E* **95** (2017).
- [18] J. Larson, B. M. Anderson, and A. Altland, *Phys. Rev. A* **87**, 013624 (2013).
- [19] O.V. Marchukov, A.G. Volosniev, D.V. Fedorov, A.S. Jensen, and N.T. Zinner, *Journal of Physics B: Atomic, Mol. and Opt. Phys.* **47**, 195303 (2014).
- [20] D. V. Khomitsky, A. I. Malyshev, E. Ya. Sherman, and M. Di Ventra, *Phys. Rev. B* **88**, 195407 (2013).
- [21] L. Chotorlishvili, Z. Toklikishvili, A. Komnik, and J. Berakdar, *J. Phys. Condens. Matter.* **24** 255302 (2012).
- [22] Yu. A. Bychkov and E.I. Rashba, *JETP Lett.* **39**, 78 (1984).
- [23] I. Žutić, J. Fabian, and S. Das Sarma, *Rev. Mod. Phys.* **76**, 323 (2004).
- [24] Although  $\alpha$  can be either positive or negative, we consider here only  $\alpha > 0$  realization.
- [25] E. N. Adams and E. I. Blount, *J. Phys. Chem. Solids* **10**, 286 (1959).
- [26] The role of the modified position operator for macroscopic spin effects in two-dimensional electron systems was studied in X. Bi, P. He, E. M. Hankiewicz, R. Winkler, G. Vignale, and D. Culcer, *Phys. Rev. B* **88**, 035316 (2013).
- [27] J. Schliemann, D. Loss, and R. M. Westervelt, *Phys. Rev. Lett.* **94**, 206801 (2005).
- [28] R. Winkler, U. Zülicke, and J. Bolte, *Phys. Rev. B* **75**, 205314 (2007).
- [29] P. Harrison and A. Valavanis, *Quantum Wells, Wires and Dots: Theoretical and Computational Physics of Semiconductor Nanostructures* (John Wiley & Sons, Ltd., 2016)
- [30] A. A. High, A. K. Thomas, G. Grosso, M. Remeika, A. T. Hammack, A. D. Meyertholen, M. M. Fogler, L. V. Butov, M. Hanson, and A. C. Gossard, *Phys. Rev. Lett.* **103**, 087403 (2009).